# Motion of an array of plates in a rarefied gas caused by radiometric force

Satoshi Taguchi*
*Department of Mechanical Engineering and Intelligent Systems, The University of Electro-Communications, Chofu, Tokyo 182-8585, Japan*

Kazuo Aoki
*Department of Mechanical Engineering and Science and Advanced Research Institute of Fluid Science and Engineering, Graduate School of Engineering, Kyoto University, Kyoto 606-8501, Japan*

(Received 6 April 2015; published 17 June 2015)

In a rarefied gas in an infinitely long channel between two parallel plates, an array of infinitely many plates, arranged longitudinally with uniform interval, is placed along the channel. The array is assumed to be freely movable along the channel. If one side of each plate is heated, the radiometric force acts on it, and the array starts moving toward the cold sides of the plates. The final steady motion of the array, as well as the corresponding behavior of the gas, is investigated numerically on the basis of kinetic theory using the ellipsoidal statistical model of the Boltzmann equation. As the solution method, a finite-difference method, with a method of characteristics incorporated, that is able to capture the discontinuity in the velocity distribution function is employed. As the result, the local flow field near the edges of the plates and the terminal velocity of the array are obtained accurately for relatively small Knudsen numbers.

DOI: 10.1103/PhysRevE.91.063007 PACS number(s): 47.45.−n, 47.61.−k, 51.10.+y

## I. INTRODUCTION

The Crookes radiometer, also known as the light mill, is a device which operates by using the rarefied gas (kinetic) effect. More specifically, it consists of a glass bulb containing a low pressure gas and a vaned wheel supported by a spindle in it. The vane wheel can rotate freely, and one side of each vane is blackened, whereas the other side is reflective (or metallic). When exposed to the light (radiation), the vanes inside the bulb start rotating in the direction toward the metallic sides. The mechanism behind the moving vanes was once of great curiosity [1–6]. The recent development of micro technologies brought again the attention of many scientists to this classical device [7–25]. The reader is referred to [18] for the history as well as for the recent studies on the radiometric phenomenon.

In our previous study [14,16], motivated by the radiometric phenomenon, we considered a simple model problem, in which a (two-dimensional) plate, without thickness and with one side heated, is placed in a rarefied gas in a square box. We investigated the steady gas flow induced around the plate and the force acting on the plate (radiometric force) numerically on the basis of kinetic theory, using the Bhatnagar-Gross-Krook (BGK) model [26,27] of the Boltzmann equation, for a wide range of the Knudsen number. In [14,16], the emphasis was put on the detailed structure of the flow field near the edges of the plate. For this purpose, we carried out an accurate numerical analysis using the method that is able to capture the discontinuity in the velocity distribution function near the edges. It was found that, in the near continuum regime (i.e., for small Knudsen numbers), the radiometric force is effectuated only in the vicinity of the edges and is attributed to the thermal stress caused by the steep temperature change near the edges.

In an actual radiometer, however, the vanes are not at rest but are moving continuously in the gas. There are some recent studies of the radiometric phenomenon for moving vanes [15,19,22,25]. These works successfully demonstrate that moving boundary problems are within reach also in kinetic theory of gases. However, there is still lack of detailed information on the structure of the flow field, such as the velocity and temperature fields and stress distribution, near the edge of a moving vane.

Therefore, in the present study, we propose a simple problem modeling the moving vanes, which is an extension of that in [16], and try to obtain some detailed information on the flow field. The model problem, which should be simple enough for accurate and detailed numerical analysis, should retain the essential feature of the moving vanes of a radiometer. To be more specific, we consider a rarefied gas in an infinitely long channel between two parallel plates and place an array of infinitely many plates, arranged longitudinally with uniform interval, along the channel. We assume that the array can move freely along the channel. If we heat one side of each plate, the radiometric force acts on it, and the array starts moving toward the cold sides of the plates. We investigate the final steady motion of the array and the corresponding behavior of the gas numerically on the basis of kinetic theory, with special interest in the local flow field near the edges of the plates and in obtaining the terminal velocity of the array. We use the ellipsoidal statistical (ES) model [28–30] of the Boltzmann equation as the basic equation. The numerical method used here is basically the same as that used in [16]. We only need small adjustments for the present problem and the ES model.

The organization of the paper is as follows. After this introduction, we state the problem and the assumptions in Sec. II. Then, we give the basic equations and boundary conditions in Sec. III. A brief remark on the numerical method is given in Sec. IV. In Sec. V, we show the results of numerical analysis. Section VI is devoted to discussions about the cause of the radiometric force, and Sec. VII to concluding remarks.

*Electronic address: taguchi.satoshi@uec.ac.jp

 

## II. PROBLEM AND ASSUMPTIONS

The problem that is considered in the present paper is described as follows:

*Problem I.* Consider a rarefied gas in a two-dimensional straight channel between two parallel walls located at $X_2 = \pm L/2$, where $X_i$ is the Cartesian coordinate system. In the channel, an array consisting of infinitely many two-dimensional flat plates without thickness, which are spaced uniformly and oriented perpendicularly to the $X_1$ axis, is placed along the $X_1$ axis [Fig. 1(a)]. The array can move freely along the $X_1$ axis. The width of each plate is denoted by $D$, and the interval between two plates by $H$. Suppose that the left surface of each plate is kept at the same temperature $T_0$ as the channel walls, whereas its right surface is kept at a higher temperature $T_1$. Then, a leftward force acts on each plate because of the temperature difference between the two surfaces (radiometric force), so that the array moves in the leftward direction. It finally reaches a steady motion with a constant velocity $(-v^*, 0, 0)$ $(v^* > 0)$ [Fig. 1(a)], in which the radiometric force acting on each plate is counterbalanced by the drag force caused by the motion of the plate in the gas. Investigate the behavior of the gas in this final state and obtain the final speed $v^*$ of the array.

We are going to analyze this problem numerically under the following assumptions:

(i) The behavior of the gas is described by the ellipsoidal statistical (ES) model [29] of the Boltzmann equation.

(ii) The gas molecules undergo diffuse reflection [31] on the plates as well as on the channel walls. More specifically, the velocity of the gas molecules reflected from the boundary is distributed according to the corresponding part (i.e., the half range) of the Maxwellian distribution characterized by the temperature and velocity of the boundary and by the condition that there is no net mass flow across the boundary.

Problem I is an unsteady problem in the whole range of the channel $(-\infty < X_1 < \infty, -L/2 < X_2 < L/2)$. However, if we take the coordinate system moving with the array, that is, moving with the velocity $(-v^*, 0, 0)$, then, the array is at rest, and the channel walls are moving with the velocity $(v^*, 0, 0)$ rightward in the new coordinate system. As is easily checked by the Galilean transformation, the latter problem in the new coordinate system is time independent. Moreover, the flow field is periodic with period $H$ in the $X_1$ direction. This simplifies the computation significantly. The only problem is that we do not know the final speed $v^*$ beforehand.

Therefore, we modify the latter time-independent problem slightly: We assume that the walls are moving with a given velocity $(v_w, 0, 0)$ $(v_w > 0)$ rightward. Then, we adjust $v_w$ in such a way that the total force acting on each plate vanishes. This $v_w$ is nothing but $v^*$. In this way, we can obtain the original speed of the array $v^*$.

To be more specific, we consider the following time-independent problem:

*Problem II.* Consider a rarefied gas in a two-dimensional straight channel between two parallel walls located at $X_2 = \pm L/2$ and moving with velocity $(v_w, 0, 0)$. There is an array of the plates at rest located at $X_1 = 0, \pm H, \pm 2H, \ldots$ [Fig. 1(b)]. The other geometrical parameters, the temperatures of the plates and walls, and assumptions (i) and (ii) are the same as Problem I. Investigate the steady behavior of the gas and the force acting on the plates. In particular, obtain the speed of the walls that vanishes the total force acting on each plate.

As mentioned above, Problem II can be analyzed only in the finite domain $-H/2 < X_1 < H/2$, $-L/2 < X_2 < L/2$ by imposing the periodic boundary condition at $X_1 = \pm H/2$. In the following, we will formulate Problem II in this finite domain.

The present approach using Problem II to solve Problem I was originally proposed in [17], where only a preliminary computation was performed. It should be mentioned that a similar coordinate transformation was used to investigate the gas flow in a radiometer with a cylindrical shape in [15]. A direct numerical simulation for a cylindrical or spherical radiometer as a moving boundary problem was carried out recently in [19,22,25].

## III. BASIC EQUATIONS FOR PROBLEM II

### A. Basic equation and boundary conditions

Let $\rho_{av}$ be the average density of the gas in the domain $-H/2 < X_1 < H/2$, $-L/2 < X_2 < L/2$ and let $p_0 = R\rho_{av}T_0$, where $R$ is the gas constant per unit mass of the gas (i.e., the Boltzmann constant divided by the mass of a molecule). In addition to the symbols already mentioned,

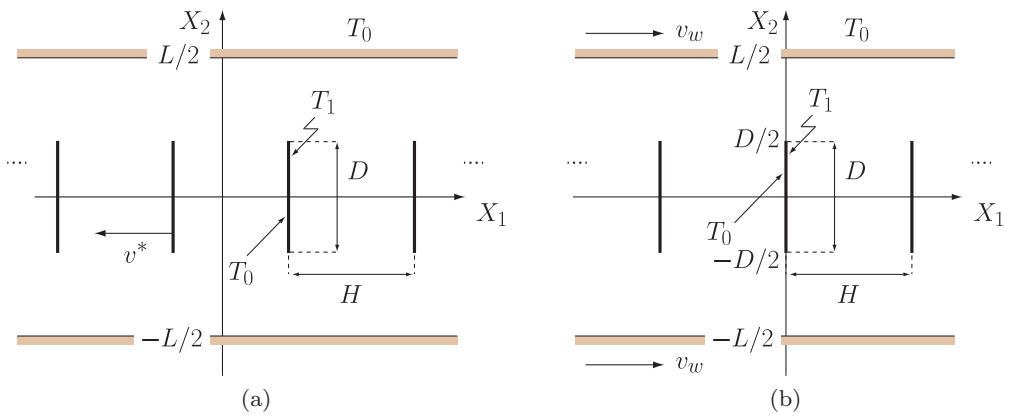


FIG. 1. (Color online) Problems I and II. (a) Problem I: An array of plates moving with velocity $(-v^*, 0, 0)$ in a gas between two walls at rest because of the radiometric force, (b) Problem II: An array of plates at rest in a gas between two walls moving with velocity $(v_w, 0, 0)$.

we introduce the following quantities: $\xi_i$ is the molecular velocity, $f(X_1, X_2, \xi_i)$ is the molecular velocity distribution function, $\rho(X_1, X_2)$ is the density of the gas, $v_i(X_1, X_2)$ is the flow velocity ($v_3 = 0$), $T(X_1, X_2)$ is the temperature, $p(X_1, X_2) = R\rho T$ is the pressure, and $p_{ij}(X_1, X_2)$ is the stress tensor ($p_{13} = p_{23} = p_{31} = p_{32} = 0$). Then, we introduce the dimensionless counterparts $(x_i, \zeta_i, \hat{f}, \hat{\rho}, \hat{v}_i, \hat{T}, \hat{p}, \hat{p}_{ij})$ of $(X_i, \xi_i, f, \rho, v_i, T, p, p_{ij})$ as follows:

$$\begin{aligned} x_i &= X_i/D, \quad \zeta_i = \xi_i/(2RT_0)^{1/2}, \\ \hat{f}(x_1, x_2, \zeta_i) &= f/[\rho_{av}(2RT_0)^{-3/2}], \\ \hat{\rho}(x_1,x_2) &= \rho/\rho_{av}, \quad \hat{v}_i(x_1,x_2) = v_i/(2RT_0)^{1/2}, \\ \hat{T}(x_1,x_2) &= T/T_0, \\ \hat{p}(x_1,x_2) &= p/p_0 = \hat{\rho}\hat{T}, \quad \hat{p}_{ij}(x_1,x_2) = p_{ij}/p_0, \end{aligned} \tag{1}$$

where $\hat{v}_3 = 0$ and $\hat{p}_{13} = \hat{p}_{23} = \hat{p}_{31} = \hat{p}_{32} = 0$.

The macroscopic quantities $\hat{\rho}$, $\hat{v}_i$, etc. are given by appropriate moments of $\hat{f}$:

$$\hat{\rho} = \int \hat{f} d\boldsymbol{\zeta}, \quad \hat{v}_i = \frac{1}{\hat{\rho}} \int \zeta_i \hat{f} d\boldsymbol{\zeta}, \tag{2a}$$

$$\hat{T} = \frac{\hat{p}}{\hat{\rho}} = \frac{2}{3\hat{\rho}} \int (\zeta_j - \hat{v}_j)^2 \hat{f} d\boldsymbol{\zeta}, \tag{2b}$$

$$\hat{p}_{ij} = 2 \int (\zeta_i - \hat{v}_i)(\zeta_j - \hat{v}_j) \hat{f} d\boldsymbol{\zeta}, \tag{2c}$$

where $d\boldsymbol{\zeta} = d\zeta_1 d\zeta_2 d\zeta_3$ and the domain of integration is the whole space of $\boldsymbol{\zeta}$.

Furthermore, we introduce the following dimensionless parameters:

$$\begin{aligned} \hat{T}_1 &= \frac{T_1}{T_0}, \quad \hat{v}_w = \frac{v_w}{(2RT_0)^{1/2}}, \\ \mathrm{Kn} &= \frac{\ell_0}{D}, \quad \hat{L} = \frac{L}{D}, \quad \hat{H} = \frac{H}{D}. \end{aligned} \tag{3}$$

Here, $\ell_0$ is the mean free path of the gas molecules at the equilibrium state at rest with density $\rho_{av}$ and temperature $T_0$, which is defined, for the ES model, as

$$\ell_0 = (2/\sqrt{\pi})(2RT_0)^{1/2}/A_c\rho_{av}, \tag{4}$$

with $A_c$ a constant such that $A_c\rho$ is the collision frequency of the gas molecules, and Kn is the Knudsen number that represents the degree of gas rarefaction.

The ES model in the present steady and spatially two-dimensional problem is written as

$$\begin{aligned} &\zeta_1 \frac{\partial \hat{f}}{\partial x_1} + \zeta_2 \frac{\partial \hat{f}}{\partial x_2} = \frac{2}{\sqrt{\pi}\mathrm{Kn}} \hat{\rho}(\mathcal{G} - \hat{f}), \\ &\left( -\frac{\hat{H}}{2} < x_1 < \frac{\hat{H}}{2}, \quad -\frac{\hat{L}}{2} < x_2 < \frac{\hat{L}}{2} \right), \end{aligned} \tag{5}$$

where

$$\mathcal{G} = \frac{\hat{\rho}}{\pi^{3/2}(\det \mathsf{A})^{1/2}} \exp\left( -\frac{1}{2} b_{ij}(\zeta_i - \hat{v}_i)(\zeta_j - \hat{v}_j) \right), \tag{6a}$$

$$\mathsf{A} = (a_{ij}), \quad a_{ij} = (1 - \nu)\hat{T}\delta_{ij} + \nu \frac{\hat{p}_{ij}}{\hat{\rho}}, \tag{6b}$$

$$b_{ij} = (i, j) \text{ component of } \mathsf{A}^{-1}, \tag{6c}$$

and $\hat{\rho}$, $\hat{v}_i$, $\hat{T}$, and $\hat{p}_{ij}$ in Eq. (6) are expressed in terms of $\hat{f}$ as given by Eq. (2). Here, $\mathsf{A}$ is the matrix whose $(i, j)$ component is given by $a_{ij}$, $\mathsf{A}^{-1}$ and $\det\mathsf{A}$ are, respectively, the inverse matrix and the determinant of $\mathsf{A}$, $\delta_{ij}$ is the Kronecker delta, and $\nu$ ($-1/2 \leqslant \nu < 1$) in Eq. (6b) is a parameter. The viscosity $\mu_0$ and the thermal conductivity $\lambda_0$ for this model at our reference state are given by $\mu_0 = (1 - \nu)^{-1} p_0/A_c\rho_{av}$ and $\lambda_0 = (5/2)Rp_0/A_c\rho_{av}$, respectively. Therefore, the Prandtl number Pr at the same state, which is defined by $\mathrm{Pr} = 5R\mu_0/2\lambda_0$, is expressed in terms of the parameter $\nu$ as $\mathrm{Pr} = 1/(1 - \nu)$. Thus, $\mathrm{Pr} = 2/3$ for $\nu = -1/2$, and $\mathrm{Pr} = 1$ for $\nu = 0$. In the latter case, Eq. (5) reduces to the BGK model.

The diffuse reflection condition on the right and left surfaces of the plate located at $x_1 = 0$ is written as

$$\begin{aligned} \hat{f} &= \frac{\hat{\sigma}_w^{\pm}}{\left(\pi \hat{T}_w^{\pm}\right)^{3/2}} \exp\left( -\frac{\zeta_j^2}{\hat{T}_w^{\pm}} \right), \quad \text{for} \pm \zeta_1 > 0, \\ &(x_1 = 0_{\pm}, \ -1/2 < x_2 < 1/2), \end{aligned} \tag{7}$$

$$\hat{\sigma}_w^{\pm} = \mp 2 \left( \frac{\pi}{\hat{T}_w^{\pm}} \right)^{1/2} \int_{\pm\zeta_1 < 0} \zeta_1 \hat{f}(x_1 = 0_{\pm}, x_2, \zeta_i) d\boldsymbol{\zeta}, \tag{8}$$

$$\hat{T}_w^{+} = \hat{T}_1, \quad \hat{T}_w^{-} = 1, \tag{9}$$

where the upper (or lower) sign corresponds to the condition on the right (or left) surface.

The diffuse reflection condition on the channel walls is given as

$$\begin{aligned} \hat{f} &= \frac{\hat{\sigma}_w}{\pi^{3/2}} \exp\left( -(\zeta_1 - \hat{v}_w)^2 + \zeta_2^2 + \zeta_3^2 \right), \\ &\text{for} \pm\zeta_2 < 0, \text{ at } x_2 = \pm\hat{L}/2, \end{aligned} \tag{10}$$

with

$$\hat{\sigma}_w = \pm 2\sqrt{\pi} \int_{\pm\zeta_2 > 0} \zeta_2 \hat{f}(x_1, \pm \hat{L}/2, \zeta_i) d\boldsymbol{\zeta}, \tag{11}$$

where the upper (or lower) signs go together.

The periodic boundary condition is applied at $x_1 = \pm\hat{H}/2$, i.e.,

$$\hat{f}(\pm\hat{H}/2, x_2, \zeta_i) = \hat{f}(\mp\hat{H}/2, x_2, \zeta_i), \quad \text{for} \pm\zeta_1 < 0, \tag{12}$$

where the upper (or lower) signs go together.

Since the problem is symmetric with respect to the $x_1$ axis, we can analyze the problem only in the upper half domain $-\hat{H}/2 < x_1 < \hat{H}/2$, $0 < x_2 < \hat{L}/2$ by imposing the specular reflection condition on the $x_1$ axis, i.e.,

$$\hat{f}(x_1,0,\zeta_1,\zeta_2,\zeta_3) = \hat{f}(x_1,0,\zeta_1, -\zeta_2,\zeta_3), \quad \text{for } \zeta_2 > 0. \tag{13}$$

In summary, the system to be solved consists of Eqs. (5)–(12), restricted to the upper half domain $0 < x_2 < \hat{L}/2$, and Eq. (13). The solution in the lower half domain is obtained from that in the upper half domain by the following relation:

$$\begin{aligned} &\hat{f}(x_1,x_2,\zeta_1,\zeta_2,\zeta_3) = \hat{f}(x_1, -x_2,\zeta_1, -\zeta_2,\zeta_3), \\ &(-\hat{L}/2 \leqslant x_2 < 0). \end{aligned} \tag{14}$$

### B. Further transformations

As in the case of the BGK model, we can eliminate the $x_3$ component of the molecular velocity $\zeta_3$ from the system of equations, following the standard procedure (i.e., the two-dimensional version of the procedure in [32]). We first introduce the marginal velocity distribution functions $g$ and $h$ and the two-component vector $\Phi$ composed of $g$ and $h$:

$$\Phi = \begin{bmatrix} g \\ h \end{bmatrix} = \int_{-\infty}^{\infty} \begin{bmatrix} 1 \\ \zeta_3^2 \end{bmatrix} \hat{f} d\zeta_3. \tag{15}$$

Then, multiplying Eqs. (5), (7), (10), and (12), restricted to the upper half domain ($0 < x_2 < \hat{L}/2$), and Eq. (13) by 1 and $\zeta_3^2$ and integrating the results with respect to $\zeta_3$ from $-\infty$ to $\infty$, we obtain a system of simultaneous equations for $g$ and $h$. The equations and boundary conditions thus obtained are summarized as follows. The equations are

$$\zeta_1 \frac{\partial \Phi}{\partial x_1} + \zeta_2 \frac{\partial \Phi}{\partial x_2} = \frac{2}{\sqrt{\pi}} \frac{1}{\mathrm{Kn}} \hat{\rho} (\Phi_g - \Phi), \tag{16a}$$

$$\Phi_g = \begin{bmatrix} 1 \\ a_{33}/2 \end{bmatrix} \frac{\hat{\rho}}{\pi (\det \overline{\mathsf{A}})^{1/2}} \times \exp\left( - \sum_{k,l=1}^{2} \overline{b}_{kl} (\zeta_k - \hat{v}_k)(\zeta_l - \hat{v}_l) \right), \tag{16b}$$

$$\hat{\rho} = \int_{-\infty}^{\infty} \int_{-\infty}^{\infty} g d\zeta_1 d\zeta_2, \tag{16c}$$

$$\hat{v}_k = \frac{1}{\hat{\rho}} \int_{-\infty}^{\infty} \int_{-\infty}^{\infty} \zeta_k g d\zeta_1 d\zeta_2 \quad (k = 1,2), \tag{16d}$$

$$\hat{T} = \frac{2}{3\hat{\rho}} \int_{-\infty}^{\infty} \int_{-\infty}^{\infty} \{ [(\zeta_1 - \hat{v}_1)^2 + (\zeta_2 - \hat{v}_2)^2] g + h \} d\zeta_1 d\zeta_2, \tag{16e}$$

$$\hat{p}_{kl} = 2 \int_{-\infty}^{\infty} \int_{-\infty}^{\infty} (\zeta_k - \hat{v}_k)(\zeta_l - \hat{v}_l) g d\zeta_1 d\zeta_2 \quad (k,l = 1,2), \tag{16f}$$

$$\hat{p}_{33} = 2 \int_{-\infty}^{\infty} \int_{-\infty}^{\infty} h d\zeta_1 d\zeta_2, \tag{16g}$$

$$\overline{\mathsf{A}} = \begin{pmatrix} a_{11} & a_{12} \\ a_{21} & a_{22} \end{pmatrix}, \tag{16h}$$

$$\overline{b}_{kl} = (k,l) \text{ component of } \overline{\mathsf{A}}^{-1}, \tag{16i}$$

with $a_{kl}$ $(k,l = 1,2)$ and $a_{33}$ being defined in Eq. (6b). The boundary condition on the right and left surfaces of the plate is

$$\Phi = \begin{bmatrix} 2/\hat{T}_w^{\pm} \\ 1 \end{bmatrix} \frac{\hat{\sigma}_w^{\pm}}{2\pi} \exp\left( - \frac{\zeta_1^2 + \zeta_2^2}{\hat{T}_w^{\pm}} \right), \quad \text{for } \pm\zeta_1 > 0, \quad (x_1 = 0_{\pm},\ 0 \leqslant x_2 \leqslant 1/2), \tag{17a}$$

$$\hat{\sigma}_w^{\pm} = \mp 2 \left( \frac{\pi}{\hat{T}_w^{\pm}} \right)^{1/2} \int_{\pm\zeta_1 < 0} \zeta_1 g(x_1 = 0_{\pm}, x_2, \zeta_1, \zeta_2) d\zeta_1 d\zeta_2, \tag{17b}$$

$$\hat{T}_w^{+} = \hat{T}_1, \quad \hat{T}_w^{-} = 1. \tag{17c}$$

The condition on the upper channel wall is

$$\Phi = \begin{bmatrix} 2 \\ 1 \end{bmatrix} \frac{\hat{\sigma}_w}{2\pi} \exp\left( - \left[ (\zeta_1 - \hat{v}_w)^2 + \zeta_2^2 \right] \right), \quad \text{for } \zeta_2 < 0, \quad (-\hat{H}/2 < x_1 < \hat{H}/2,\ x_2 = \hat{L}/2), \tag{18a}$$

$$\hat{\sigma}_w = 2\sqrt{\pi} \int_{\zeta_2 > 0} \zeta_2 g(x_1, \hat{L}/2, \zeta_1, \zeta_2) d\zeta_1 d\zeta_2. \tag{18b}$$

The periodic condition on the side boundary and the specular reflection on the $x_1$ axis are, respectively,

$$\Phi(\pm\hat{H}/2, x_2, \zeta_1, \zeta_2) = \Phi(\mp\hat{H}/2, x_2, \zeta_1, \zeta_2), \quad \text{for } \pm\zeta_1 < 0, \quad (0 < x_2 < \hat{L}/2), \tag{19}$$

$$\Phi(x_1, 0, \zeta_1, \zeta_2) = \Phi(x_1, 0, \zeta_1, -\zeta_2), \quad \text{for } \zeta_2 > 0, \quad (-\hat{H}/2 < x_1 < \hat{H}/2). \tag{20}$$

As is seen from Eqs. (16a), (17a), (18a), (19), and (20), the present problem is characterized by the five dimensionless parameters listed in Eq. (3). In addition, Eq. (16a) contains an adjustable parameter $\nu$ through $a_{33}$ and $\overline{b}_{kl}$ [cf. Eq. (16h)]. In the present study, we set $\nu = -1/2$, so that $\mathrm{Pr} = 2/3$.

## IV. NUMERICAL METHOD: A BRIEF REMARK

We solve the boundary-value problem, Eqs. (16a)–(20), basically by the finite-difference method. The numerical method employed in the present study is essentially the same as that in [16]. Therefore, the reader is referred to [16]. Here, we only give a brief remark on the numerical method.

As pointed out in [33] (see also [31]), the velocity distribution function of the gas molecules contains discontinuities in the gas around a convex body. The convexity of the body concentrates on the edges of the plate in the problem under consideration. On the other hand, discontinuous boundary data, such as a discontinuous boundary temperature, also induce discontinuities in the velocity distribution function in the gas (see [34,35]), irrespective of the shape of the boundary. This cause for the discontinuity is also located on the edges of the plate in the present problem.

Numerical methods that are able to describe the above mentioned discontinuity have been developed in Kyoto University [34,36–39], and the method used in [16] and here is based on these methods, in particular, the method in [39], where a problem containing sharp edges is considered.

The procedure is outlined in Appendix A of [16]. The essential point is that, for each discretized molecular velocity, say $(\zeta_1^{(k)}, \zeta_2^{(l)})$, the velocity distribution function $\Phi$, as the function of $(x_1, x_2)$, is generally discontinuous along the straight line originating from the (upper) edge of the plate and parallel to the vector $(\zeta_1^{(k)}, \zeta_2^{(l)})$. For $\zeta_2^{(l)} > 0$, it is also discontinuous along the part for $x_2 > 0$ of the straight line originating from the lower edge and parallel to $(\zeta_1^{(k)}, \zeta_2^{(l)})$ [it is the reflection on the $x_1$ axis of the line originating from the upper edge parallel to $(\zeta_1^{(k)}, -\zeta_2^{(l)})$]. We divide the domain $-\hat{H}/2 < x_1 < \hat{H}/2, 0 < x_2 < \hat{L}/2$ by the lines of discontinuity and apply the finite-difference formula in each subdomain in order to avoid the finite-difference approximation across the line of discontinuity. In this procedure, for each discretized

$(\zeta_1^{(k)}, \zeta_2^{(l)})$, the limiting values of $\Phi$ on both sides of the line of discontinuity are required as the boundary condition for each subdomain. We prepare these limiting values beforehand by solving Eq. (16a) along both sides of the discontinuity line (characteristic line) using finite-difference approximation. In short, the method is a combination of the finite-difference method and the method of characteristics.

However, there is an important difference between the present problem and the problem of [16]. In the latter problem, a single plate is placed in a gas in a closed domain bounded by the wall with diffuse reflection. Therefore, when the discontinuity line reaches the wall, it is absorbed there and is never transmitted to the gas again. In other words, the number of the discontinuity lines is at most two for each $(\zeta_1^{(k)}, \zeta_2^{(l)})$. In contrast, in the present problem, the discontinuity line that reaches one of the periodic boundaries ($x_1 = \pm\hat{H}/2$) is transmitted to the gas through the other periodic boundary. Therefore, when $0 < \zeta_2^{(l)} \ll 1$, many discontinuity lines cross over the gas region (infinitely many as $\zeta_2^{(l)} \to 0$). However, the discontinuity decays over the distance of the order of Kn from the edge of the plate along the discontinuity line. Therefore, if we consider the case where the Knudsen number is relatively small (say, Kn $\lesssim 0.5$), we can safely ignore the discontinuities transmitted through the periodic boundaries. Thus, by doing so, our scheme becomes almost exactly the same as that used in [16].

Concerning the numerical results that will be presented in the next section, we will also omit the descriptions about the used grid systems and the accuracy of the results. Since they are similar to those in [16], we just refer the reader to this reference for the details. It should be emphasized, however, that the accuracy in the present computation is of the same level as or higher than that in [16].

## V. RESULTS OF NUMERICAL ANALYSIS

The first step of our analysis is to solve Problem II to obtain the flow field and the force acting on the plate for a given set of the parameters $(\hat{T}_1, \hat{v}_w, \text{Kn}, \hat{L}, \hat{H})$ [cf. Eq. (3)]. The second step is to change $\hat{v}_w$ for the fixed $(\hat{T}_1, \text{Kn}, \hat{L}, \hat{H})$ in Problem II and find its value $\hat{v}^* = v^*/(2RT_0)^{1/2}$ for which the net force acting on the plate vanishes. This solves the original Problem I.

In the present paper, we show the results for $\hat{L} = \hat{H} = 4$ and $\hat{T}_1 = 2$, unless otherwise stated [e.g., Fig. 3, Table I, and Fig. 17(b) contain other cases]. We mainly show the solution of Problem I in the coordinate system moving with the plates, or equivalently, the solution of Problem II for $\hat{v}_w = \hat{v}^*$. However, we also present some results of Problem II for assigned values of $\hat{v}_w$ (cf. Secs. V A, V C, V F, and VI).

### A. Force acting on the plate in Problem II

We first give an example that shows the behavior of the net force acting on the plate when the velocity of the wall $\hat{v}_w$ is changed in Problem II. Figure 2 shows the net force $(F_1, 0, 0)$ acting on the plate (per unit length in the $X_3$ direction), normalized by $p_0 D$, versus $v_w/(2RT_0)^{1/2} (= \hat{v}_w)$ for Kn $= 0.1$, 0.2, 0.3, and 0.5. It is seen from the figure that it is not difficult to find $\hat{v}_w$ that vanishes the net force by several trials. In the actual computation, instead of performing the two steps mentioned at the beginning of Sec. V separately, we also solve Problem I directly by carrying out the adjustment of $\hat{v}_w$ in the process of iteration in such a manner that the magnitude of the total force acting on the plate tends to decrease.

TABLE I. Terminal speed of the array $v_*$ vs Kn in Problem I ($L/D = 4$).

| | $v_*/(2RT_0)^{1/2} \times 10^2$ | | |
|---|---|---|---|
| | $T_1/T_0 = 2$ | $T_1/T_0 = 2$ | $T_1/T_0 = 1.5$ |
| Kn | $H/D = 4$ | $H/D = 2$ | $H/D = 4$ |
| 0.05 | 2.385 | 2.654 | 1.181 |
| 0.06 | 2.617 | 2.913 | 1.300 |
| 0.07 | 2.804 | 3.136 | 1.400 |
| 0.08 | 2.995 | 3.331 | 1.489 |
| 0.09 | 3.149 | 3.504 | 1.569 |
| 0.1 | 3.317 | 3.617 | 1.667 |
| 0.15 | 3.826 | 4.225 | 1.945 |
| 0.2 | 4.165 | 4.683 | 2.142 |
| 0.3 | 4.584 | 5.266 | 2.390 |
| 0.4 | 4.826 | 5.646 | 2.540 |
| 0.5 | 4.981 | 5.915 | 2.640 |

### B. Speed of the array $v^*$ in Problem I

In this subsection, we show one of the main results, that is, the final velocity of the array in Problem I. In Fig. 3, $v^*$ of the final velocity $(-v^*, 0, 0)$ is shown versus the Knudsen number for $L/D = 4$: • indicates the result for $T_1/T_0 = 2$, $H/D = 4$, ○ that for $T_1/T_0 = 2$, $H/D = 2$, and ◇ that for $T_1/T_0 = 1.5$, $H/D = 4$. The corresponding numerical values of $v^*$ is shown in Table I. Since $(2RT_0)^{1/2}$ is a quantity of the order of the sound speed, $v^*/(2RT_0)^{1/2}$ is roughly the Mach number of the motion of the array. When $T_1/T_0 = 1.5$ and Kn $= 0.1$, it becomes 0.0167, which is not small at all in our daily experience.

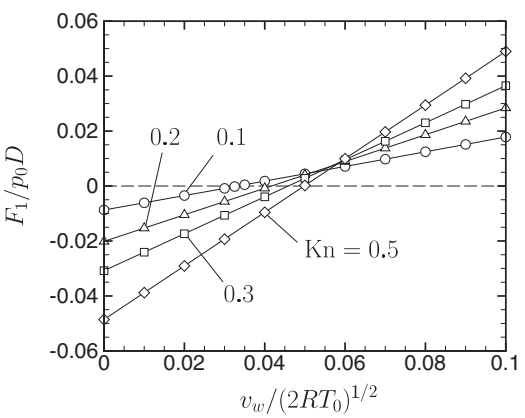


FIG. 2. Net force $F_1/p_0D$ vs $v_w/(2RT_0)^{1/2}$ in Problem II for several Kn in the case of $T_1/T_0 = 2$ ($L/D = H/D = 4$). The numerical results are shown by the symbols. The dashed line indicates $F_1 = 0$.

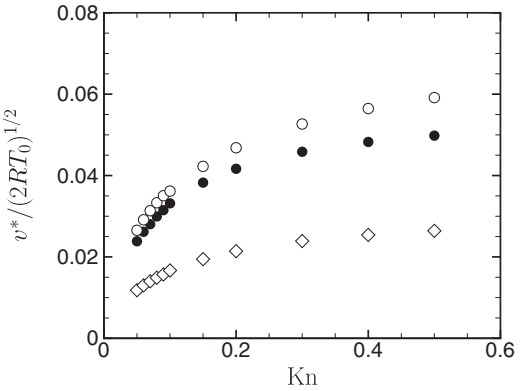


FIG. 3. Terminal speed of the array $v^*$ vs Kn in Problem I ($L/D = 4$). Here, • indicates the result for $T_1/T_0 = 2$, $H/D = 4$, ○ that for $T_1/T_0 = 2$, $H/D = 2$, and ◇ that for $T_1/T_0 = 1.5$, $H/D = 4$.

### C. Flow field

Next, we show the flow field when $v_w = v^*$ in Problem II for two Knudsen numbers, Kn = 0.5 and 0.05. This is nothing but the flow field of the solution of Problem I seen by the observer moving with the plate. To see the effect of the motion of the plate, we also show the corresponding results when $v_w = 0$ in Problem II. Because of the symmetry, only the upper half ($X_2 > 0$) of the flow field is shown in the figures in this subsection.

Figure 4 shows the flow velocity field $(v_1, v_2)$ for Kn = 0.5 [(a) and (c)] and 0.05 [(b) and (d)] in the case of $T_1/T_0 = 2$ ($L/D = H/D = 4$). The upper figures [(a) and (b)] are for $v_w = v^*$ in Problem II (or Problem I), and the lower figures [(c) and (d)] for $v_w = 0$ in Problem II. In the figures, the arrow indicates the flow velocity vector $(v_1, v_2)/(2RT_0)^{1/2}$ at its starting point, and the scale is indicated at the top right corner of each figure. The first and second quadrants are separated slightly to show the flow velocity on the plate clearly. In order to see the detailed velocity field near the edge, we show in Fig. 5 the magnified figures around the edge corresponding to Fig. 4. Since the wall is moving in Figs. 4(a) and 4(b) and is at rest in Figs. 4(c) and 4(d), the flow velocity field near the wall in Fig. 4(a) [or Fig. 4(b)] is different from that in Fig. 4(c) [or Fig. 4(d)]. However, the flow velocity near the plate in Fig. 5(a) [or Fig. 5(b)] does not differ much from that in Fig. 5(c) [or Fig. 5(d)]. This is due to the fact that $\hat{v}^*$ is relatively small [$\hat{v}^* \simeq 0.050$ for panel (a) in Figs. 4 and 5 and $\hat{v}^* \simeq 0.024$ for panel (b) in these figures]. The difference whether the plate is moving with the velocity $(-v^*, 0, 0)$ or at rest can be observed more clearly in Fig. 6, where the isolines of the flow speed $|v_i|/(2RT_0)^{1/2} = \text{const}$ are depicted. Figures 6(a)–6(d) correspond to the cases of Figs. 4(a)–4(d), respectively.

In Figs. 7–9, we show the isolines of the density $\rho/\rho_{av} = \text{const}$, those of the temperature $T/T_0 = \text{const}$, and those of the pressure $p/p_0 = \text{const}$. Panels (a)–(d) in these figures correspond to the cases of Figs. 4(a)–4(d), respectively. The difference between panel (a) and panel (c) and that between panel (b) and panel (d) are very small in Figs. 7 and 8. That is, the density and temperature fields are little affected by whether the plate is moving with the velocity $(-v^*, 0, 0)$ or at rest. Therefore, the same should be true for the pressure field. However, the difference between Figs. 9(a) and 9(c) and that between Figs. 9(b) and 9(d) are significant. This is due to the fact that the variation of pressure over the flow field is small, especially for small Kn [Figs. 9(b) and 9(d)], so that the small difference is exaggerated in the figure of isobaric lines. One should note, however, that this small difference in pressure (more precisely, the small difference in the normal stress $p_{11}$) results in whether or not the net force acting on

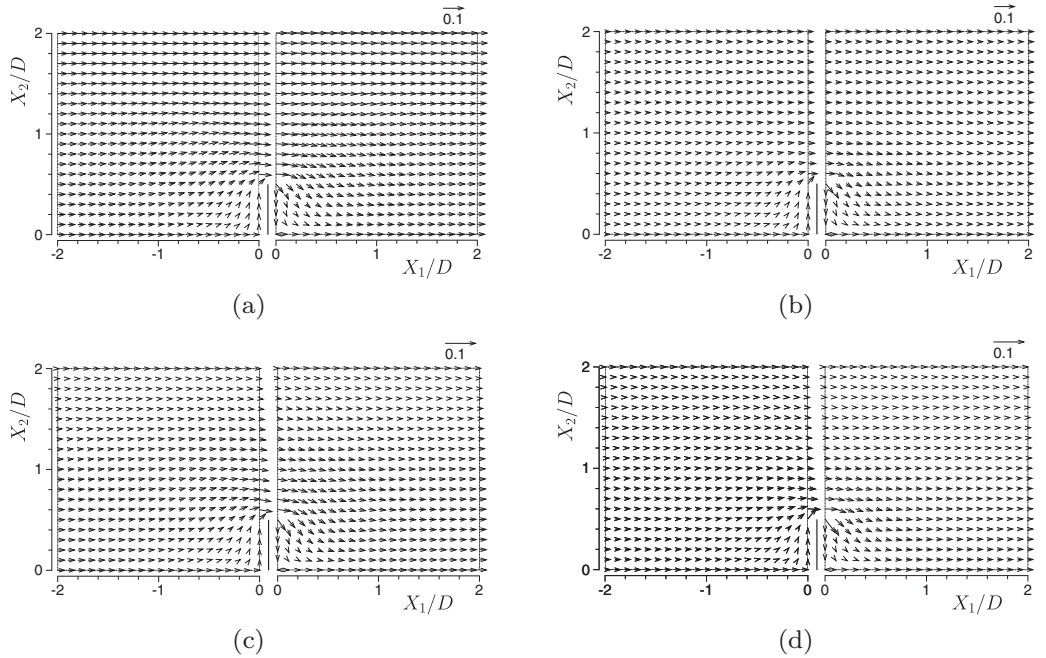


FIG. 4. Flow velocity field $(v_1, v_2)$ in the case of $T_1/T_0 = 2$ ($L/D = H/D = 4$). (a) Kn = 0.5 (Problem I, or $v_w = v^*$ in Problem II); (b) Kn = 0.05 (Problem I, or $v_w = v^*$ in Problem II); (c) Kn = 0.5 ($v_w = 0$ in Problem II); (d) Kn = 0.05 ($v_w = 0$ in Problem II). The arrow indicates the flow velocity vector $(v_1, v_2)/(2RT_0)^{1/2}$ at its starting point, and the scale is shown at the top right corner of each figure.

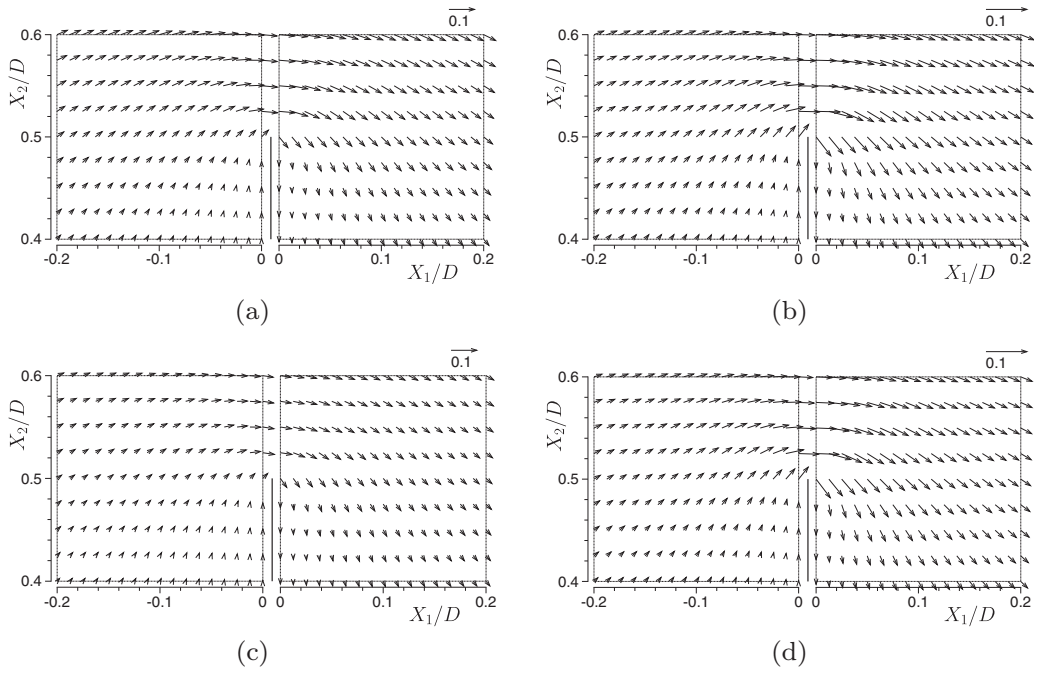


FIG. 5. Magnified figure of the flow velocity field near the edge in the case of $T_1/T_0 = 2$ ($L/D = H/D = 4$). (a) Kn $= 0.5$ (Problem I, or $v_w = v^*$ in Problem II); (b) Kn $= 0.05$ (Problem I, or $v_w = v^*$ in Problem II); (c) Kn $= 0.5$ ($v_w = 0$ in Problem II); (d) Kn $= 0.05$ ($v_w = 0$ in Problem II). See the caption of Fig. 4.

the plate vanishes. Figures 6–9 (in particular, Figs. 7 and 8) demonstrate that the isolines concentrate on the edge. In other words, the macroscopic quantities are singular there in the sense that they do not take a unique value there. This singularity is described correctly only by the precise description of the discontinuity in the velocity distribution function, as shown in the next subsection.

### D. Velocity distribution function

In Figs. 10 and 11, we show the marginal velocity distribution functions $g$ and $h$ [cf. Eq. (15)] seen by the observer moving with the plate in Problem I (or equivalently, $g$ and $h$ when $v_w = v^*$ in Problem II). Figure 10 is for Kn $= 0.5$ and Fig. 11 for Kn $= 0.05$ in the case of $T_1/T_0 = 2$

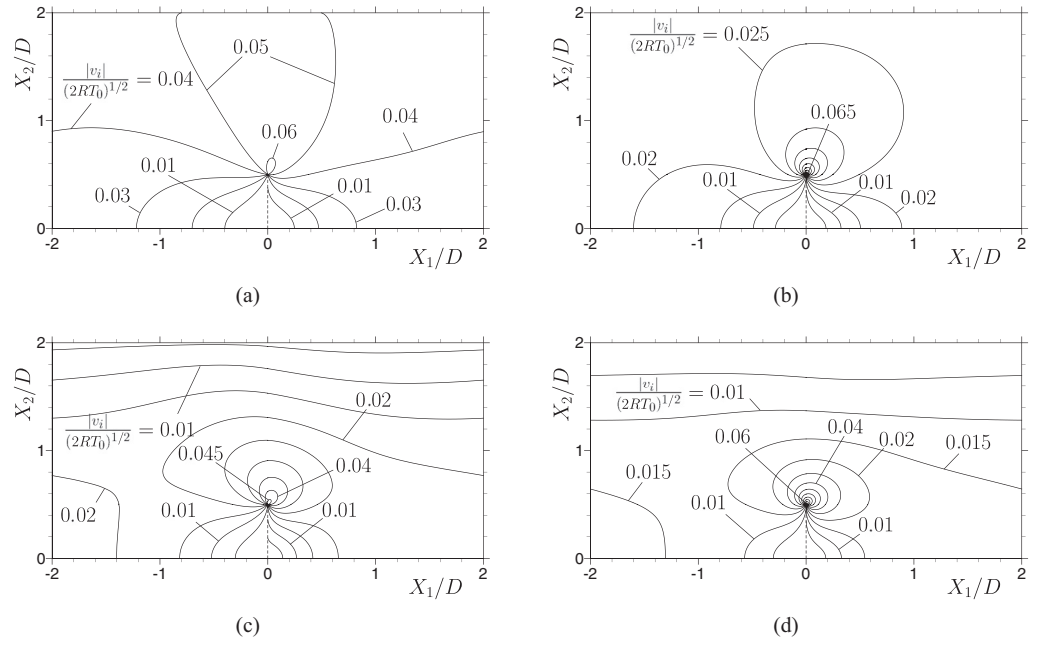


FIG. 6. Isolines of the flow speed $|v_i|/(2RT_0)^{1/2} = \text{const}$ in the case of $T_1/T_0 = 2$ ($L/D = H/D = 4$). (a) Kn $= 0.5$ (Problem I, or $v_w = v^*$ in Problem II), $|v_i|/(2RT_0)^{1/2} = 0.01 + 0.01m$ ($m = 0, \ldots, 5$); (b) Kn $= 0.05$ (Problem I, or $v_w = v^*$ in Problem II), $|v_i|/(2RT_0)^{1/2} = 0.005 + 0.005m$ ($m = 0, \ldots, 12$); (c) Kn $= 0.5$ ($v_w = 0$ in Problem II), $|v_i|/(2RT_0)^{1/2} = 0.005 + 0.005m$ ($m = 0, \ldots, 8$); (d) Kn $= 0.05$ ($v_w = 0$ in Problem II), $|v_i|/(2RT_0)^{1/2} = 0.005 + 0.005m$ ($m = 0, \ldots, 12$).

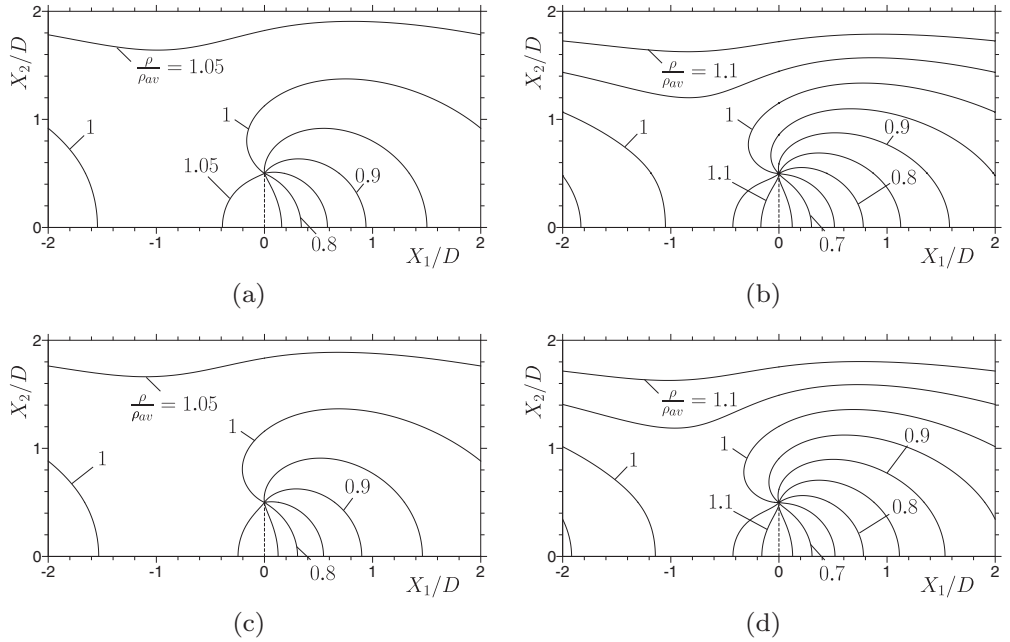


FIG. 7. Isolines of the density $\rho/\rho_{av} = \text{const}$ in the case of $T_1/T_0 = 2$ ($L/D = H/D = 4$). (a) Kn $= 0.5$ (Problem I, or $v_w = v^*$ in Problem II), $\rho/\rho_{av} = 0.75 + 0.05m$ ($m = 0, \ldots, 6$); (b) Kn $= 0.05$ (Problem I, or $v_w = v^*$ in Problem II), $\rho/\rho_{av} = 0.65 + 0.05m$ ($m = 0, \ldots, 9$); (c) Kn $= 0.5$ ($v_w = 0$ in Problem II), $\rho/\rho_{av} = 0.75 + 0.05m$ ($m = 0, \ldots, 6$); (d) Kn $= 0.05$ ($v_w = 0$ in Problem II), $\rho/\rho_{av} = 0.65 + 0.05m$ ($m = 0, \ldots, 9$).

($L/D = H/D = 4$). The figures show $g$ and $h$ as functions of $\zeta_1$ and $\zeta_2$ at four points along the line $x_2\ (= X_2/D) = 0.5$: $(X_1/D, X_2/D) = (-0.05, 0.5)$ [(a)], $(0.05, 0.5)$ [(b)], $(0.5, 0.5)$ [(c)], and $(1, 0.5)$ [(d)]. When the Knudsen number is not small (Fig. 10), the discontinuity originating from the upper edge is observed clearly along the line $\zeta_2 = 0$ in both $g$ and $h$ at the points near the edge [Figs. 10(a) and 10(b)]. But, the discontinuity originating from the lower edge, which has almost decayed, can barely be observed in Fig. 10(b) (along $\zeta_2 = -20\zeta_1$). Since the corresponding discontinuity is

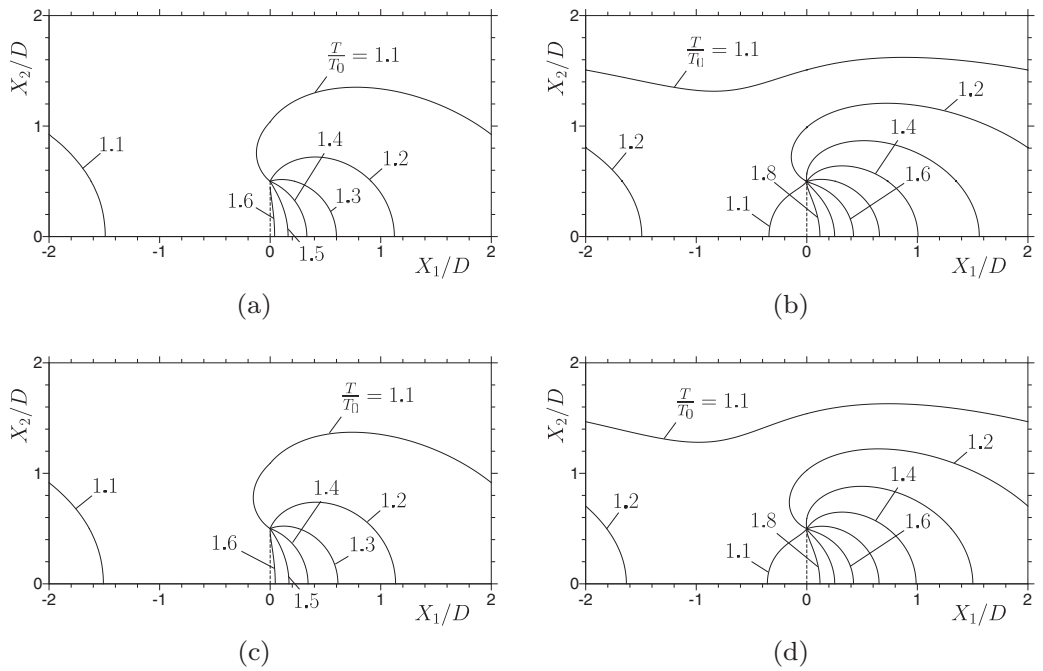


FIG. 8. Isolines of the temperature $T/T_0 = \text{const}$ in the case of $T_1/T_0 = 2$ ($L/D = H/D = 4$). (a) Kn $= 0.5$ (Problem I, or $v_w = v^*$ in Problem II), $T/T_0 = 1.1 + 0.1m$ ($m = 0, \ldots, 5$); (b) Kn $= 0.05$ (Problem I, or $v_w = v^*$ in Problem II), $T/T_0 = 1.1 + 0.1m$ ($m = 0, \ldots, 7$); (c) Kn $= 0.5$ ($v_w = 0$ in Problem II), $T/T_0 = 1.1 + 0.1m$ ($m = 0, \ldots, 5$); (d) Kn $= 0.05$ ($v_w = 0$ in Problem II), $T/T_0 = 1.1 + 0.1m$ ($m = 0, \ldots, 7$).

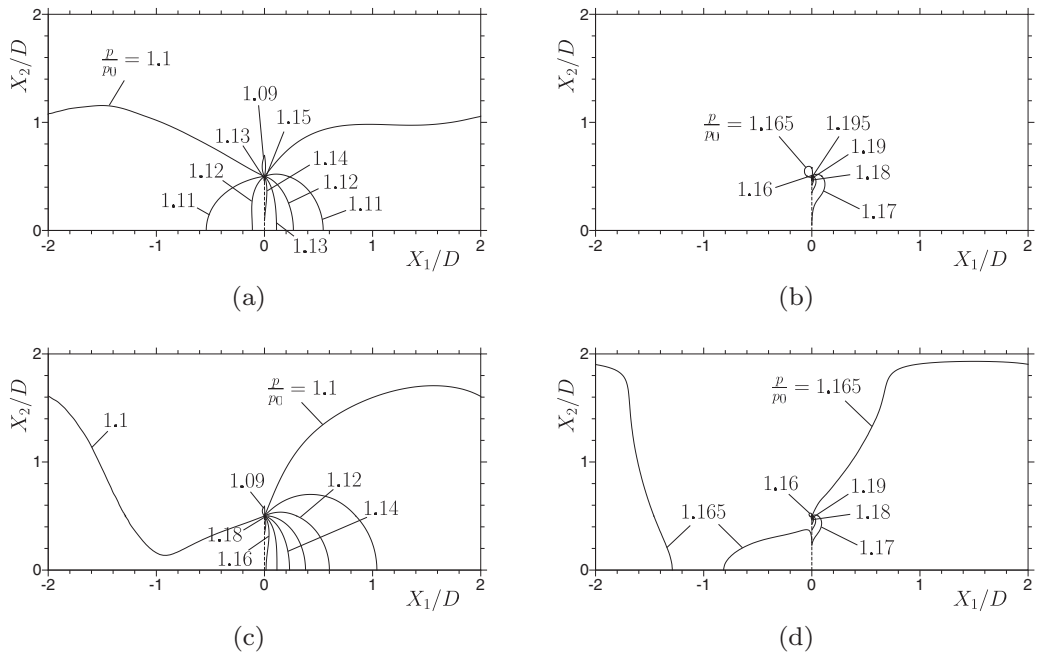


FIG. 9. Isolines of the pressure $p/p_0 = \text{const}$ in the case of $T_1/T_0 = 2$ ($L/D = H/D = 4$). (a) Kn = 0.5 (Problem I, or $v_w = v^*$ in Problem II), $p/p_0 = 1.09 + 0.01m$ ($m = 0, \ldots, 6$); (b) Kn = 0.05 (Problem I, or $v_w = v^*$ in Problem II), $p/p_0 = 1.16 + 0.005m$ ($m = 0, \ldots, 7$); (c) Kn = 0.5 ($v_w = 0$ in Problem II), $p/p_0 = 1.09 + 0.01m$ ($m = 0, \ldots, 9$); (d) Kn = 0.05 ($v_w = 0$ in Problem II), $p/p_0 = 1.16 + 0.005m$ ($m = 0, \ldots, 7$).

on the other side of the "mountain" in Fig. 10(a) [note that the directions of the $\zeta_1$ and $\zeta_2$ axes in Fig. 10(a) are different from those in Figs. 10(b)–10(d)], it is invisible. As the distance from the upper edge increases [Fig. 10(b) → Fig. 10(c) → Fig. 10(d)], even the discontinuity produced by it decays and is almost invisible in Fig. 10(d). When the Knudsen number is relatively small (Fig. 11), the discontinuity caused by the upper edge is barely visible even at the points close to the edge [Figs. 11(a) and 11(b)] and is already invisible in Fig. 11(c). It should be noted, however, that even for this Knudsen number, $g$ and $h$ are similar to Figs. 10(a) and 10(b) at the points $(X_1/D, X_2/D) = (-0.005, 0.5)$ and $(0.005, 0.5)$ that are a half-mean-free path apart from the edge. The limiting location of the discontinuity in $g$ and $h$ as the edge is approached depends on the direction of approach. This fact is reflected as the singularity in the macroscopic quantities mentioned in the last part of Sec. V C.

As noted in the fifth paragraph in Sec. IV, we have neglected the discontinuities originating from the edges of the neighboring plates. In fact, when Kn $\lesssim 0.5$, their effect is practically invisible. On the other hand, as was noted in the last paragraph in Sec. V C, even small changes are well visible in the isobaric lines in Fig. 9 because the variation in the pressure is small. This means that a small computational error might be magnified and become appreciable in the isobaric lines. It is true, and even the computation that is accurate enough gives a slightly fluctuating isobaric line for $p/R\rho_{av}T_0 = 1.1$ between $X_1/D = -1$ and $-2$ when $v_w = 0$ and Kn = 0.5. The reason why such fluctuations are not observed in Fig. 9(c) is that we showed there the result with higher accuracy, based on a very fine grid system, than other cases.

### E. Normal stress on the plate

In the solution of Problem I, the net force acting on the plate vanishes. However, how the local force is distributed along the plate is not obvious. In this subsection, we look into the stress distribution on the plate as well as in the gas. Here again, we consider the stress distribution only in the upper half ($X_2 > 0$) because of the symmetry of the problem.

Figures 12 and 13 show the distribution of the normal stress $p_{11}/p_0$ along the lines $X_1/D = \text{const}$ parallel and close to the plate for Kn = 0.5 (Fig. 12) and 0.05 (Fig. 13) in the case of $T_1/T_0 = 2$ ($L/D = H/D = 4$), as seen by the observer moving with the plate in Problem I. In each figure, panel (a) shows the distribution along the vertical lines located in the left side of the plate (including the line along the left surface of the plate, $X_1/D = 0_-$), whereas panel (b) that along the vertical lines in the right side of the plate (including the line along the right surface of the plate, $X_1/D = 0_+$). The change in $p_{11}$ is sharp near the edge and is discontinuous at the edge along the plate ($X_1/D = 0_\pm$).

On the plate, let us put $p_{11}^- = p_{11}(X_1 = 0_-, X_2)$ and $p_{11}^+ = p_{11}(X_1 = 0_+, X_2)$. Then, $p_{11}^-$ indicates the rightward (positive $X_1$) component of the local force acting on the unit area of the left surface of the plate at point $(0_-, X_2)$, and $p_{11}^+$ the leftward (negative $X_1$) component of the local force acting on the unit area of the right surface of the plate at point $(0_+, X_2)$. Therefore, the difference $[p_{11}]_+^- = p_{11}^- - p_{11}^+$ is the rightward (positive $X_1$) component of the local force acting on the unit area of the plate at point $(0, X_2)$. Figure 14(a) shows the distributions of $p_{11}^-$ and $p_{11}^+$ along (the upper half of) the plate for different Kn in the case of $T_1/T_0 = 2$ ($L/D = H/D = 4$), and Fig. 14(b) the distribution of the difference $[p_{11}]_+^-$ in the same case. Roughly speaking, the

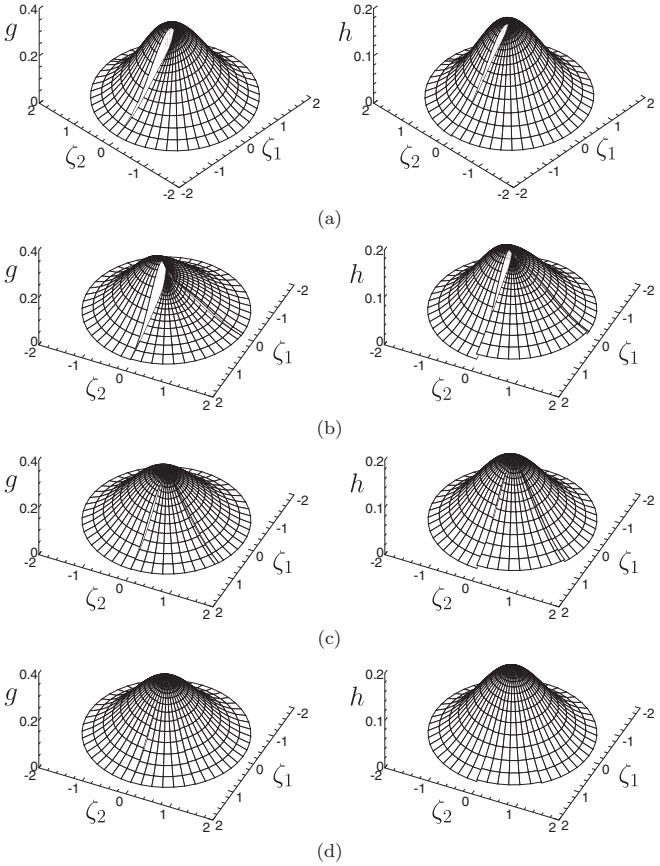


FIG. 10. Marginal velocity distribution functions $g$ and $h$ for $\mathrm{Kn} = 0.5$ in the case of $T_1/T_0 = 2$ $(L/D = H/D = 4)$ (Problem I). (a) $(X_1/D, X_2/D) = (-0.05, 0.5)$; (b) (0.05, 0.5); (c) (0.5, 0.5); (d) (1, 0.5).

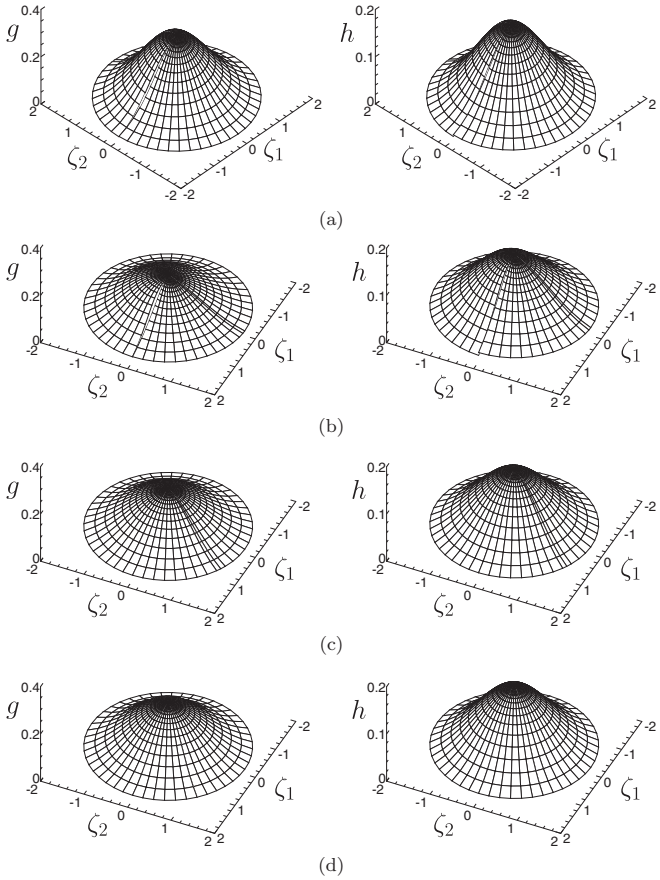


FIG. 11. Marginal velocity distribution functions $(g,h)$ for $\mathrm{Kn} = 0.05$ in the case of $T_1/T_0 = 2$ $(L/D = H/D = 4)$ (Problem I). (a) $(X_1/D, X_2/D) = (-0.05, 0.5)$; (b) (0.05, 0.5); (c) (0.5, 0.5); (d) (1, 0.5).

positive $[p_{11}]_+^-$ is attributed to the drag force caused by the motion of the plate, whereas the negative $[p_{11}]_+^-$ to the effect of the temperature difference (radiometric effect). For an intermediate Kn ($\mathrm{Kn} = 0.5$), $[p_{11}]_+^-$ is negative in the middle of the plate but is positive near the edge. However, as Kn decreases, the distribution becomes opposite. The physical reasoning of this phenomenon will be discussed in Sec. VI.

### F. Pumping effect of the array fixed in space

Finally, we discuss the potential pumping effect when the array of the plates is fixed in the channel. More specifically, we consider Problem II with the resting channel walls ($v_w = 0$), some results of which have already been shown in panels (c) and (d) in Figs. 4–9. As seen from these figures, a one-way flow in the rightward (positive $X_1$) direction is induced in the channel in spite of the fact that both the array and the channel walls are at rest. In other words, this setting can be a variant of the Knudsen compressor or pump that has been studied extensively (e.g., [40–48]). Let $M_f$ be the net mass flow of the gas in the (positive) $X_1$ direction, per unit time and per unit length in the $X_3$ direction, across any cross section $X_1 = \mathrm{const}$ (say, the periodic boundary $X_1 = H/2$). In Fig. 15, the mass-flow rate $M_f$ through the channel, normalized by $\rho_{av}(2RT_0)^{1/2}D$, is shown versus Kn for three different geometries $(H/D, L/D) = (4, 4)$, $(2, 4)$, and $(4, 2)$ in the case of $T_1/T_0 = 2$. Here, we have carried out additional computations using the DSMC method for hard sphere molecules and show the results together with those based on the ES model. In Fig. 15, • indicates the result based on the ES model, and the open symbols (□, △, and ◇) indicate the result for hard-sphere molecules obtained by the DSMC method. The same results are shown in Table II, where the DSMC results are shown in the parentheses. The mass-flow rate takes its maximum value at a relatively small Kn (0.1–0.3).

## VI. DISCUSSIONS: CAUSE OF THE RADIOMETRIC FORCE

The usual explanation about the cause of the radiometric force is as follows. Let us consider a plate placed in a gas as shown in Fig. 16(a) and suppose that one side (right side) of the plate is heated, that is, it is kept at a higher temperature than the other side (left side) and the surrounding gas. The molecules hitting on the unheated surface are reflected with the same average speed as before, whereas the molecules hitting on the heated surface interact with the molecules of the surface with the higher temperature and are reflected with a higher average speed. That is, the molecules reflected on the heated surface gain momentum in the rightward direction in Fig. 16(a). This

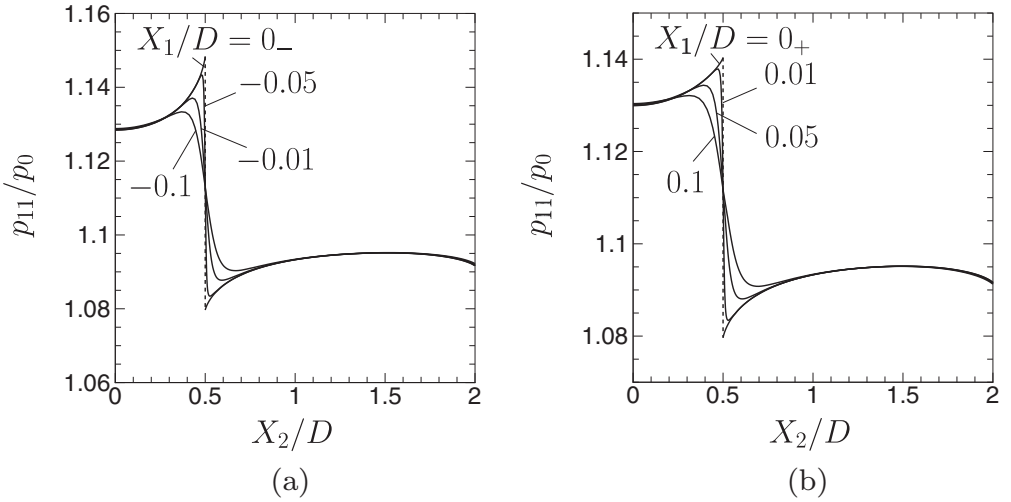


FIG. 12. Distributions of the normal stress $p_{11}/p_0$ along $X_1/D = \text{const}$ for Kn = 0.5 in the case of $T_1/T_0 = 2$ ($L/D = H/D = 4$) (Problem I). (a) $X_1/D = 0_-$, −0.01, −0.05, and −0.1; (b) $X_1/D = 0_+$, 0.01, 0.05, and 0.1.

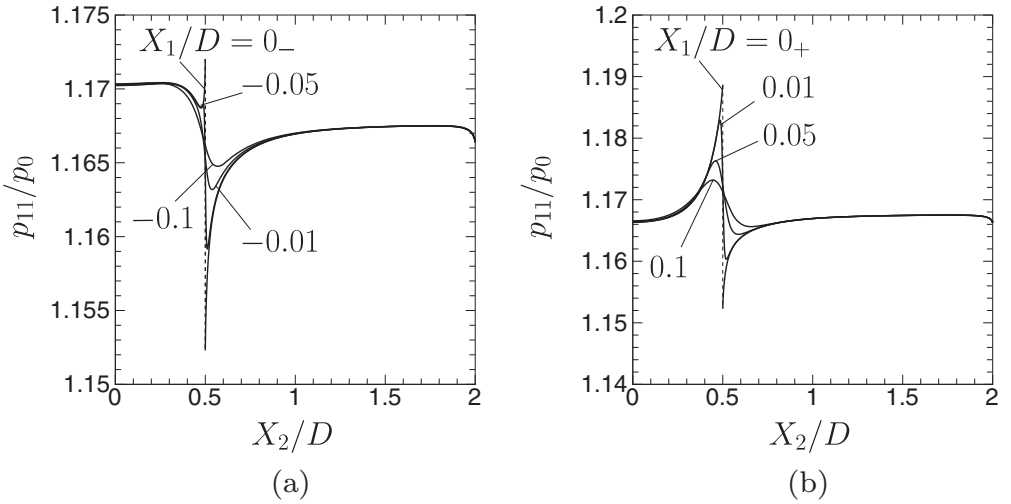


FIG. 13. Distributions of the normal stress $p_{11}/p_0$ along $X_1/D = \text{const}$ for Kn = 0.05 in the case of $T_1/T_0 = 2$ ($L/D = H/D = 4$) (Problem I). (a) $X_1/D = 0_-$, −0.01, −0.05, and −0.1; (b) $X_1/D = 0_+$, 0.01, 0.05, and 0.1.

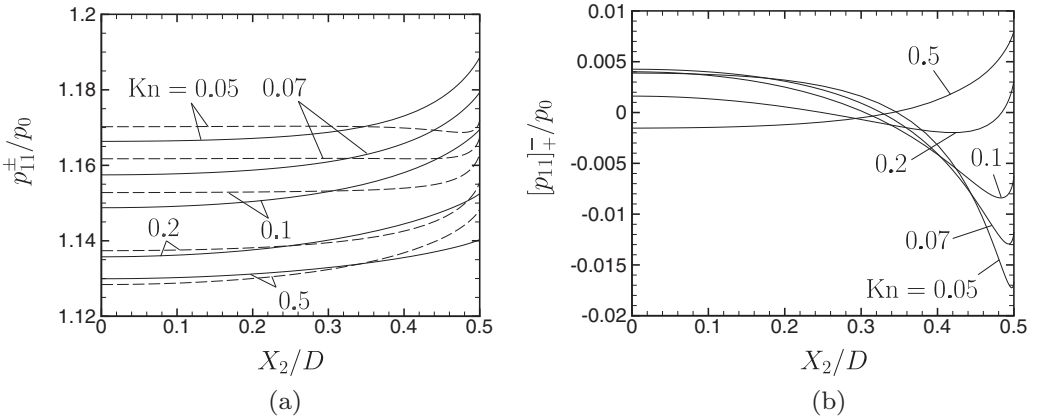


FIG. 14. Distributions of the normal stress along each side of the plate for different Kn in the case of $T_1/T_0 = 2$ ($L/D = H/D = 4$) (Problem I). (a) $p_{11}^- = p_{11}(X_1 = 0_-, X_2)$ and $p_{11}^+ = p_{11}(X_1 = 0_+, X_2)$; (b) $[p_{11}]_+^- = p_{11}^- - p_{11}^+$. In (a), $p_{11}^+$ is shown by the solid line and $p_{11}^-$ by the dashed line.

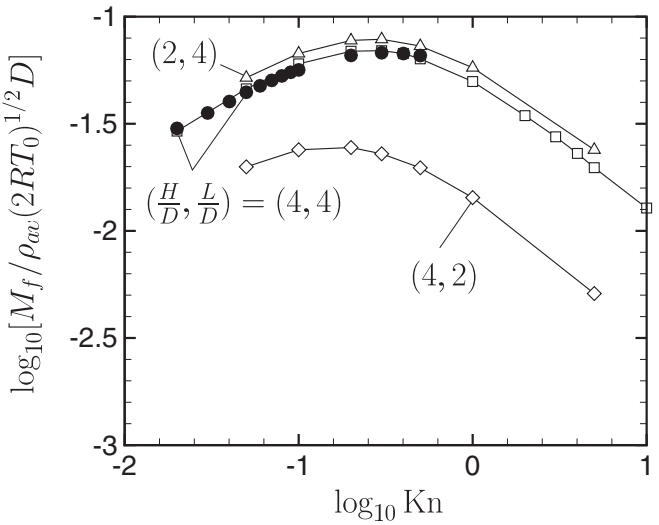


FIG. 15. Dimensionless mass flow rate $M_f/\rho_{av}(2RT_0)^{1/2}D$ through the channel vs Kn for a stationary array ($v_w = 0$) in the case of $T_1/T_0 = 2$ (Problem II). Here, • indicates the result based on the ES model, and the open symbols (□, △, and ◇) connected by the solid lines indicate the results for hard-sphere molecules obtained by the DSMC method.

means that the plate gains the momentum in the leftward direction, so that a force in this direction acts on the plate.

This explanation is correct when collisions between the gas molecules are not frequent. If the Knudsen number is infinitely large (the free-molecular gas), and the condition for the incident molecules is the same on both sides of the plate, then, according to the explanation, the local force acting on the plate should be uniform over the plate. This tendency should be retained also at finite Knudsen numbers.

However, if the collisions are frequent, i.e., if the Knudsen number is small, the molecules reflected on the heated surface collide with other incident molecules immediately after the reflection. Since the reflected molecules have larger rightward momentum, they hit the incident molecules away from the plate [Fig. 16(b)]. As the result, the number of molecules impinging on the heated surface is reduced. This reduction reduces the total leftward momentum transferred to the plate by the molecules reflected on the heated surface. In the continuum limit (Kn → 0), the reduction of the number of the incident molecules on the heated surface cancels the increase of the leftward momentum caused by the molecules (with high average speed) reflected on the heated surface. As the result, no force acts on the plate in this limit. When the Knudsen number is small but finite, these two effects do not cancel exactly but nearly cancel. Therefore, the force acting on the plate is expected to be quite small. However, if we look at the part near the edge [Fig. 16(c)], the situation is different. Also in this part, the molecules with larger rightward momentum reflected on the heated surface collide with the incident molecules and hit them back rightward. However, the molecules impinging on the part of the hot surface near the edge from above are less bombarded by the high-speed molecules reflected on the hot surface because there is no plate above the edge. Therefore, the number of the incident molecules from above is less reduced by the reflected molecules with higher speed. As the result, the total number of the incident molecules is less reduced near the edge than in the middle part of the plate. In other words, when Kn is small, the mechanism explained in the first paragraph works only near the edge of the plate, so that the radiometric force acts more strongly there.

In order to verify the above explanation, we have prepared Fig. 17(a), which shows the normal component of the local force, $[p_{11}]^-_+ = p^-_{11} - p^+_{11}$, along the plate when $v_w = 0$ in Problem II [cf. Fig. 14(b)]. In this problem, the condition of the incident molecules is different depending on the sides. The cold side faces to the gas that is heated by the hot side of the neighboring plate located leftward, whereas the hot side faces to the unheated gas. Nevertheless, when Kn is not so small (Kn = 0.5), the distribution of $[p_{11}]^-_+$ is relatively uniform, that is, it shows the tendency for large Kn explained above. Furthermore, when Kn is small (Kn = 0.02), $[p_{11}]^-_+$, which is quite small in the middle of the plate, takes larger negative values as the edge is approached. This is also consistent with the explanation above. In the present study, our computation has been restricted to relatively small Knudsen numbers (Kn ⩽ 0.5) for the reason mentioned in Sec. IV. The reader is also referred to Fig. 26(b) in [16], where we considered a single plate with one side heated, placed in a gas confined in a square box with a uniform temperature. In the figure, one can find the distribution of the local force along the plate for larger and smaller Knudsen numbers that are consistent with the explanation given above [note that $[p_{11}]^+_-$ (Ref. [16]) $= -[p_{11}]^-_+$ (present paper)].

Next, we consider the case where the plate is moving because of the radiometric force, i.e., the case in which the

TABLE II. Mass flow rate $M_f$ in the case of $T_1/T_0 = 2$ when the array is at rest [$v_w/(2RT_0)^{1/2} = 0$]. The values in the parentheses are the corresponding result for a hard sphere gas obtained by the DSMC method.

| | $M_f/\rho_{av}(2RT_0)^{1/2}D \times 10^2$ | | | |
|---|---|---|---|---|
| | $(H/D, L/D)$ | | | |
| Kn | (4,4) | | (2,4) | (4,2) |
| 0.02 | 3.009 | (2.92) | | |
| 0.03 | 3.551 | | | |
| 0.04 | 4.015 | | | |
| 0.05 | 4.436 | (4.60) | (5.19) | (1.99) |
| 0.06 | 4.753 | | | |
| 0.07 | 5.040 | | | |
| 0.08 | 5.287 | | | |
| 0.09 | 5.501 | | | |
| 0.1 | 5.643 | (6.02) | (6.73) | (2.39) |
| 0.2 | 6.593 | (6.90) | (7.75) | (2.45) |
| 0.3 | 6.784 | (6.94) | (7.84) | (2.29) |
| 0.4 | 6.728 | (6.73) | | |
| 0.5 | 6.583 | (6.35) | (7.29) | (1.97) |
| 1 | | (4.98) | (5.78) | (1.43) |
| 2 | | (3.45) | | |
| 3 | | (2.75) | | |
| 4 | | (2.30) | | |
| 5 | | (1.97) | (2.39) | (0.51) |
| 10 | | (1.28) | | |

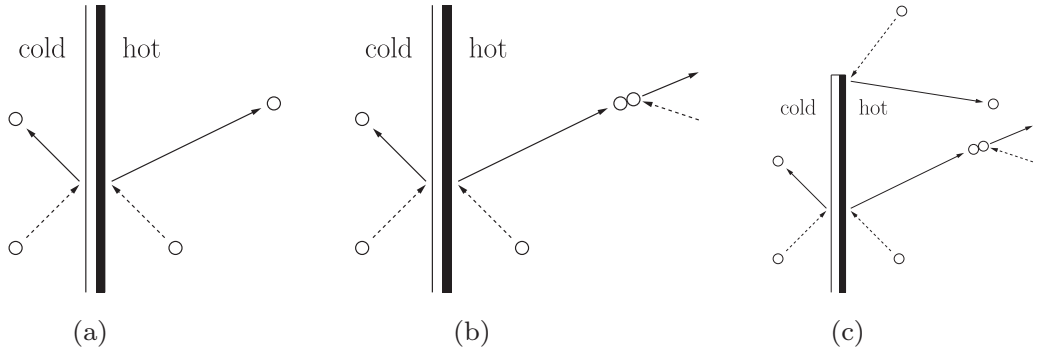


FIG. 16. Illustrative figures explaining the cause of the radiometric force. (a) High-speed molecules reflected on the heated surface, (b) high-speed molecules hitting the incident molecules away, (c) near the edge.

channel walls are moving with speed $v_w = v^*$ rightward in Problem II. If the channel walls are moving with a given speed, and if there is no temperature difference between the two surfaces of the plate, the plate is subject only to the drag force exerted by the gas moving with the walls. The gas flow speed is higher near the moving walls because the flow is obstructed by the array of the plates in the middle of the channel. Therefore, the normal component of the local force $[p_{11}]_+^-$, which should be positive, is larger near the edge. An example of the distribution of $[p_{11}]_+^-$ in such a case, i.e., for $T_1/T_0 = 1$ and $v_w/(2RT_0)^{1/2} = 0.05$ in the case of $L/D = H/D = 4$ in Problem II, is shown in Fig. 17(b). Since $v_w/(2RT_0)^{1/2} = 0.05$ is relatively small, the distribution of $[p_{11}]_+^-$ for other small $v_w/(2RT_0)^{1/2}$ can be obtained approximately by the linear scale change from Fig. 17(b). More specifically, if $v_w/(2RT_0)^{1/2} = s$, then $[p_{11}]_+^-$ in this case becomes $(s/0.05) \times [p_{11}]_+^-$ of Fig. 17(b), approximately. Now, we note that the distribution of the local force $[p_{11}]_+^-$ in Problem II with $v_w = v^*$ [see Fig. 14(b)] is roughly the superposition of $[p_{11}]_+^-$ in the case of $T_1/T_0 = t\ (> 1)$ and $v_w = 0$ [cf. Fig. 17(a)] and that in the case of $T_1/T_0 = 1$ and $v_w/(2RT_0)^{1/2} = s\ (> 0)$ [cf. Fig. 17(b)] when the total force acting on the plate vanishes. Therefore, the behavior of Fig. 14(b) can be interpreted with the help of Figs. 17(a) and 17(b). When Kn is not small (Kn = 0.5), $[p_{11}]_+^-$ in Fig. 17(a), which is negative, is relatively uniform, whereas that in Fig. 17(b), which is positive, exhibits a sharper change near the edge (compare the gradients of the curves at the edge). If these distributions are superposed in such a way that the total force vanishes, then, the radiometric effect should be stronger in the middle part of the plate, whereas the drag force should be dominant near the edge. This explains the distribution of $[p_{11}]_+^-$ when Kn is not small in Fig. 14(b). When Kn is small (Kn = 0.05), the radiometric effect is very weak in the middle of the plate, so that the drag force is dominant there. In contrast, the sharp increase of the radiometric force near the edge overwhelms the drag force there, so that the distribution of $[p_{11}]_+^-$ becomes opposite, as seen in Fig. 14(b).

In the present study, the diffuse reflection condition is used for the plates as well as for the channel walls [see assumption (ii) in the statement of Problem I in Sec. II]. If we assume Maxwell's diffuse-specular reflection condition on the plates, the radiometric force will be reduced because specularly reflected molecules do not contribute to the radiometric force. That is, the radiometric force becomes weaker as the number of specularly reflected molecules increase, i.e., as the accommodation coefficient decreases. However, the drag acting on the plates moving in the gas does not depend much on the accommodation coefficient (in the present problem the drag is independent of the tangential stress on the plate). Therefore, the speed of the motion of the plates should be lower for smaller accommodation coefficients.

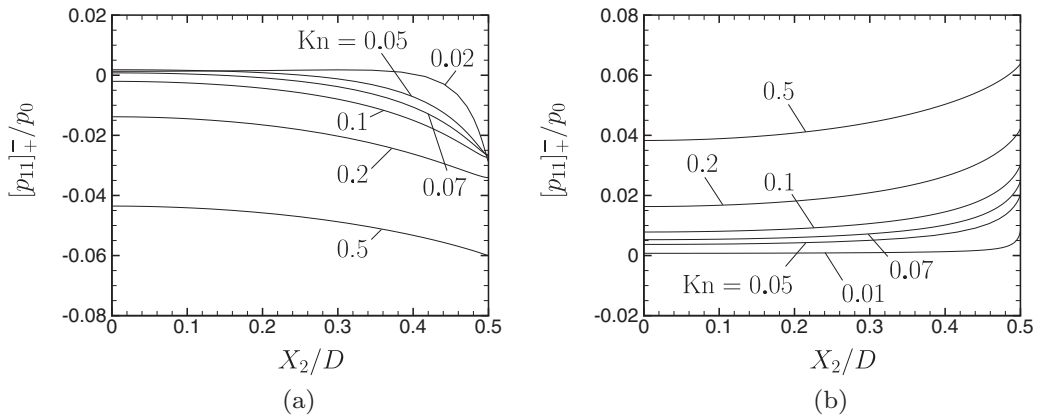


FIG. 17. Distribution of the normal component of the local force $[p_{11}]_+^-$ along the plate for several Kn ($L/D = H/D = 4$) (Problem II). (a) $T_1/T_0 = 2$ and $v_w/(2RT_0)^{1/2} = 0$, (b) $T_1/T_0 = 1$ and $v_w/(2RT_0)^{1/2} = 0.05$.

## VII. CONCLUDING REMARKS

In the present study, motivated by the moving vanes in the Crookes radiometer, we considered the motion of an array of infinitely many plates driven by the radiometric force. More specifically, we considered a rarefied gas between two parallel plates and an array of infinitely many two-dimensional plates, each of which is perpendicular to the channel walls, is placed in the gas along the channel. We supposed that the array can move freely along the channel and that the same side of each plate is heated. Then, the force caused by the temperature difference (radiometric force) acts on each plate in the direction from the heated side to the unheated side, so that the array moves toward this direction. We investigated this problem numerically on the basis of the ES model of the Boltzmann equation with special interest in the final steady motion of the array, in which the radiometric force acting on each plate is counterbalanced by the drag force acting on the plate. We first obtained the speed of the array in this case in Secs. V A and V B. Then, we investigated the corresponding flow field in Sec. V C and the velocity distribution function in Sec. V D. We also presented the flow field when the array is at rest for comparison in Sec. V C and paid attention to the discontinuity in the velocity distribution function in Sec. V D. The distribution of the normal stress as well as that of the normal component of the local force along the plate was obtained in Sec. V E. In Sec. V F, on the other hand, the one-way flow of the gas caused when the array is fixed in space was investigated, since this setting provides a potential variant of the Knudsen pump. Finally, in Sec. VI, we discussed the cause of the radiometric force physically and gave a physical interpretation of the result for the distribution of the local force along the plate shown in Sec. V E.

## ACKNOWLEDGMENTS

This work was partially supported by the AYAME Program between JSPS and Inria. The authors express their gratitude to both institutions for their support and to Professor T. Goudon and Professor F. Filbet for valuable discussions and kind hospitalities during the authors' visits to Nice and Lyon. The first author (S.T.) is grateful to Mr. Q. Guo for his help in carrying out DSMC computations. The second author (K.A.) wishes to thank Institute for Mathematical Sciences, National University of Singapore for its support and hospitality during the preparation of this paper.

[1] E. H. Kennard, *Kinetic Theory of Gases* (McGraw-Hill, New York, 1938).
[2] L. B. Loeb, *Kinetic Theory of Gases*, 3rd ed. (Dover, New York, 1961).
[3] A. Schuster, Philos. Trans. R. Soc. London **166**, 715 (1876).
[4] O. Reynolds, Philos. Trans. R. Soc. London **166**, 725 (1876).
[5] J. C. Maxwell, Philos. Trans. R. Soc. London **170**, 231 (1879).
[6] A. Einstein, Z. Phys. **27**, 1 (1924).
[7] M. Ota, T. Nakao, and M. Sakamoto, Math. Comput. Simul. **55**, 223 (2001).
[8] A. Passian, R. J. Warmack, T. L. Ferrell, and T. Thundat, Phys. Rev. Lett. **90**, 124503 (2003).
[9] M. Scandurra, F. Iacopetti, and P. Colona, Phys. Rev. E **75**, 026308 (2007).
[10] N. Selden, C. Ngalande, S. Gimelshein, E. P. Muntz, A. Alexeenko, and A. Ketsdever, Phys. Rev. E **79**, 041201 (2009).
[11] N. P. Selden, N. E. Gimelshein, S. F. Gimelshein, and A. D. Ketsdever, in *Rarefied Gas Dynamics*, edited by T. Abe (AIP, Melville, NY, 2009), pp. 1009–1014.
[12] N. P. Selden, S. F. Gimelshein, E. P. Muntz, A. Alexeenko, and A. D. Ketsdever, in *Rarefied Gas Dynamics* (Ref. [11]), pp. 959–964.
[13] N. Selden, C. Ngalande, N. Gimelshein, S. Gimelshein, and A. Ketsdever, J. Fluid Mech. **634**, 419 (2009).
[14] S. Taguchi and K. Aoki, in *27th International Symposium on Rarefied Gas Dynamics*, edited by D. A. Levin, I. J. Wysong, and A. L. Garcia (AIP, Melville, NY, 2011), pp. 790–795.
[15] Y. A. Anikin, Comput. Math. Math. Phys. **51**, 1923 (2011).
[16] S. Taguchi and K. Aoki, J. Fluid Mech. **694**, 191 (2012).
[17] S. Taguchi and K. Aoki, in *28th International Symposium on Rarefied Gas Dynamics*, edited by M. Mareschal and A. Santos (AIP, Melville, NY, 2012), pp. 786–793.
[18] A. Ketsdever, N. Gimelshein, S. Gimelshein, and N. Selden, Vacuum **86**, 1644 (2012).
[19] S. Chen, K. Xu, and C. Lee, Phys. Fluids **24**, 111701 (2012).
[20] A. Ventura, N. Gimelshein, S. Gimelshein, and A. Ketsdever, J. Fluid Mech. **735**, 684 (2013).
[21] K. Aoki, S. Takata, and T. Tomota, J. Fluid Mech. **748**, 712 (2014).
[22] G. Dechriste and L. Mieussens, in *Proceedings of the 29th International Symposium on Rarefied Gas Dynamics*, AIP Conf. Proc. No. 1628, edited by J. Fan (AIP, Melville, NY, 2014), p. 988.
[23] A. L. Ventura, A. D. Ketsdever, N. E. Gimelshein, and S. F. Gimelshein, in *Proceedings of the 29th International Symposium on Rarefied Gas Dynamics* (Ref. [22]), p. 346.
[24] A. D. Strongrich, W. J. O'Neill, A. G. Cofer, and A. A. Alexeenko, Vacuum **109**, 405 (2014).
[25] G. Dechristé and L. Mieussens, arXiv:1503.04544.
[26] P. L. Bhatnagar, E. P. Gross, and M. Krook, Phys. Rev. **94**, 511 (1954).
[27] P. Welander, Ark. Fys. **7**, 507 (1954).
[28] L. H. Holway, Jr., Ph.D. thesis, Harvard University, 1963.
[29] J. Holway, Phys. Fluids **9**, 1658 (1966).
[30] P. Andries, P. L. Tallec, J.-P. Perlat, and B. Perthame, Eur. J. Mech. B/Fluids **19**, 813 (2000).
[31] Y. Sone, *Molecular Gas Dynamics: Theory, Techniques, and Applications* (Birkhäuser, Boston, 2007), Supplementary Notes and Errata: Kyoto University Research Information Repository (http://hdl.handle.net/2433/66098).
[32] C. K. Chu, Phys. Fluids **8**, 12 (1965).
[33] Y. Sone and S. Takata, Transp. Theory Stat. Phys. **21**, 501 (1992).
[34] K. Aoki, S. Takata, H. Aikawa, and F. Golse, Phys. Fluids **13**, 2645 (2001); **13**, 3843(E) (2001).

[35] K. Aoki, C. Bardos, C. Dogbe, and F. Golse, Math. Models Methods Appl. Sci. **11**, 1581 (2001).
[36] H. Sugimoto and Y. Sone, Phys. Fluids A **4**, 419 (1992).
[37] Y. Sone and H. Sugimoto, in *Aerothermochemistry of Spacecraft and Associated Hypersonic Flows: Proceedings of the IUTAM Symposium Marseille 1992*, edited by R. Brun and A. A. Chikhaoui (Jouve, Paris, 1994), p. 67.
[38] S. Takata, Y. Sone, and K. Aoki, Phys. Fluids A **5**, 716 (1993).
[39] K. Aoki, K. Kanba, and S. Takata, Phys. Fluids **9**, 1144 (1997).
[40] M. Knudsen, Ann. Phys. **336**, 205 (1909).
[41] M. Knudsen, Ann. Phys. **338**, 1435 (1910).
[42] Y. Sone, Y. Waniguchi, and K. Aoki, Phys. Fluids **8**, 2227 (1996).
[43] S. E. Vargo and E. P. Muntz, in *Rarefied Gas Dynamics*, edited by C. Shen (Peking University Press, Beijing, 1997), pp. 995–1000.
[44] Y. Sone and H. Sugimoto, in *Rarefied Gas Dynamics*, edited by A. D. Ketsdever and E. P. Muntz (AIP, Melville, NY, 2003), pp. 1041–1048.
[45] Y. L. Han, M. Young, E. P. Muntz, and G. Shiflett, in *Rarefied Gas Dynamics*, edited by M. Capitelli (AIP, Melville, NY, 2005), p. 162.
[46] K. Aoki, P. Degond, S. Takata, and H. Yoshida, Phys. Fluids **19**, 117103 (2007).
[47] S. Taguchi, Phys. Fluids **22**, 102001 (2010).
[48] S. An, N. Gupta, and Y. Gianchandani, J. Microelectromech. S. **23**, 406 (2014).